Estimation of Percolation Flux from Borehole Temperature Data at Yucca Mountain, Nevada

G.S. Bodvarsson [a*], E. Kwicklis [b], C. Shan [a], Y. S. Wu [a]

[a] Lawrence Berkeley National Laboratory, Earth Sciences Division, 1 Cyclotron Road, MS 90-1116, Berkeley, California 94720, U.S.A.

[b] Los Alamos National Laboratory, P.O. Box 1663, Los Alamos, New Mexico 87545, U.S.A.

Abstract

Temperature data from the unsaturated zone (UZ) at Yucca Mountain are analyzed to estimate percolation-flux rates and overall heat flux. A multilayer, one-dimensional analytical solution is presented for determining percolation flux from temperature data. Case studies have shown that the analytical solution agrees very well with results from the numerical code, TOUGH2. The results of the analysis yield percolation fluxes in the range from 0 to 20 mm/yr for most of the deep boreholes. This range is in good agreement with the results of infiltration studies at Yucca Mountain. Percolation flux for the shallower boreholes, however, cannot be accurately determined from temperature data alone because large gas flow in the shallow system alters the temperature profiles. Percolation-flux estimates for boreholes located near or intersecting major faults are significantly higher than those for other boreholes. These estimates may be affected by gas flow in the faults.

* Corresponding author. Fax: +1-510-486-5686; e-mail: gsbodvarsson@lbl.gov

Key Words: Percolation flux, infiltration rate, heat flow, geothermal gradient, unsaturated zone, and Yucca Mountain.

1. Introduction

Temperature data have been collected from more than 40 boreholes in the unsaturated zone at Yucca Mountain (Sass et al., 1988; Rousseau et al., 1999). The temperature data show significant variability owing to various factors, including variabilities in thermal conductivities, thicknesses of geological formations with different thermal properties, differences in percolation fluxes near the boreholes, lateral flow of percolating water near the boreholes, and differences in the prevailing heat flux. In addition, there are problems with the temperature measurements themselves, especially the older data set from Sass et al. (1988), resulting from measurement errors, scarcity of measurements, disequilibrium between the borehole and the surrounding rock, and convective gas and water flows in the unsaturated and saturated portions of the boreholes, respectively.

The first comprehensive analysis of the temperature and thermal-conductivity data from Yucca Mountain was conducted by Sass et al. (1988), who estimated the heat flux by thermal conduction. These investigators found a significant heat-flux deficit in both the saturated zone and the thick UZ. They attributed the UZ deficit to either energy uptake by water percolating through the mountain (see the theory originally proposed by Bredehoeft and Papadopulus, 1965) or evaporation of deep waters and subsequent discharge of

warm, moist air to the atmosphere. Relatively old gas ages (on the order of thousands of years—Yang et al., 1996) for the Topopah Spring unit suggest that the percolating-water hypothesis is the more likely explanation. Rousseau et al. (1999) applied a conductive and convective model (TOUGH2) to temperature data from boreholes UZ#4 and UZ#5, and found significant variability in the inferred percolation flux.

The temperature data have been analyzed within the context of the UZ model (e.g., Bodvarsson et al. (1996). They included both conductive and convective heat-transfer methods in an attempt to infer estimates for the percolation flux through the Topopah Spring and Calico Hills formations. Bodvarsson et al. (1996) results suggested that a percolation flux of about 5–10 mm/yr in the Topopah Spring unit exist throughout most of the current repository area with somewhat lower values estimated throughout the Calico Hills Formation. The difference in percolation-flux estimates for the two units is attributed to lateral flow above the low-permeability zeolitic tuffs of the Calico Hills Formation. Sass and Lauchenbruch (1982) analyzed the percolation flux near borehole G-1 and estimated it to be 8 mm/yr, similar to the above estimates. One advantage of the method of estimating percolation flux by temperatures is that this approach is insensitive to the partitioning of the total percolation flux between fractures and the matrix, which is at present poorly known. The present study is limited to the UZ and does not explicitly consider the underlying saturated zone at Yucca Mountain.

In this paper, we perform an analysis of the temperature data using additional tools and methods. First, we review an analytical solution for conductive and convective heat flow.

Next, we apply the solution to analyzing all of the temperature data. This leads to estimates of percolation flux for all of the boreholes considered and located at different parts of the mountain. This information is crucial because percolation flux is difficult to determine and has a large impact on the performance of the potential repository, with performance inversely related to the flux rate. Finally, we utilize the numerical code TOUGH2 to check the analytical solutions and present some results of three-dimensional heat flow simulations.

2. Temperature and Heat Flow Data

Subsurface temperature was monitored in 35 test boreholes near Yucca Mountain and in particular repeated temperature logs were obtained from 18 of the 35 boreholes (Sass et al., 1988). Among them, we selected 25 boreholes, including all the boreholes with measured temperature data from the unsaturated zone within or near the site-scale model area, as shown in Figure 1. Also shown in Figure 1 is the location of most of selected boreholes. Table 1 provides coordinates and completion information for the 25 original and 7 newly drilled temperature boreholes, including UZ#5, UZ-7a, NRG-6, NRG-7a, and SD-12. Most temperature data in Table 1 were obtained from Sass et al. (1988); for the new wells, temperature data were obtained from Rousseau et al. (1999).

Temperature data from the new boreholes are thought to represent actual rock-mass temperatures more accurately because they were measured with long-term monitoring equipment that were sealed to prevent gas circulation. Temperatures reported by Sass et

al. (1988) were obtained from open, gas-filled boreholes or in sealed, water-filled tubing suspended in open boreholes. Temperatures measured in boreholes containing convecting fluids may differ significantly from actual wall-rock temperatures. However, for borehole UZ-1, the largest-diameter (about 35 centimeters) borehole at Yucca Mountain, temperatures measured by Sass et al. (1988) in the open hole, were similar to those by Rousseau et al. (1999) after the hole was instrumented, sealed, and allowed to stabilize. We have examined the temperature data (Saas et al., 1988) against the new measurements for the same boreholes. We found, in general, that the difference between these measurements is within 0.5°C, which indicates that the data from Sass et al. (1988) adequately represent *in situ* geothermal conditions for the purpose of this analysis.

Sass et al. (1988) estimated the conductive heat flow at the Yucca Mountain site based on temperature surveys and thermal conductivity measurements in both the saturated zone and the UZ. They found that heat flows in the UZ vary in a systematic fashion, both spatially and as a function of UZ thickness. The average heat flow from the UZ was evaluated to be about 41 mW/m^2 (see Figure 2). In comparison, the limited temperature data available for the saturated zone indicate an average heat flux of some 50 mW/m^2 (Sass et al., 1988; Rousseau et al., 1999). The UZ heat flux may have been influenced by processes in the UZ or the underlying saturated zone. In any case, the scatter in the saturated zone heat flux is of sufficient magnitude such that the difference between the saturated zone and UZ heat flow is not statistically significant. On the other hand, the alluvium, where exists, plays a significant role in controlling the near-surface thermal gradient or heat flow (Rousseau et al., 1999). In this study, however, effects of the

alluvium on deep heat flow are not included, because little information on steady-state infiltration can be derived from the shallow temperature data due to transient effects of surface or near-surface processes, such as evapotranspiration and seasonal climate changes.

The Yucca Mountain site is near the southern boundary of a regional heat-flow anomaly, the Eureka Low. As indicated by Sass et al. (1988), average heat flow in the Eureka Low is about half that for the adjacent regions. Fridrich et al. (1994) suggested two related interpretations for the heat-flow anomaly under Yucca Mountain. The first possible interpretation is that the anomaly may result from cool underflow in the deep carbonate aquifer (also proposed by Sass et al., 1988). The second possible interpretation is that the anomaly may be related to the zone of an apparent steep potentiometric gradient in the northern part of Yucca Mountain, suggesting that the effective northern limit of the deep carbonate aquifer (and by inference, the zone of downwelling fluid) may coincide with the large lateral potentiometric gradient under Yucca Mountain. It should be noted, however, that this steep potentiometric gradient may appear to exist because measurements of hydraulic head in perched water have been misinterpreted to represent hydraulic heads in the regional groundwater system (see Wu et al., 1998). The heat flow values within the general UZ site-scale model domain range from 35 to 45 mW/m^2, as shown in Figure 2. The contours of the figure show low heat flow in the central portion and increasing heat flow away from the center of the site-scale model area.

3. Analytical Model and Solution

Shan and Bodvarsson (2001) derived analytical expressions for the integration of temperature data; here we briefly describe the solution. The following assumptions are made: (1) water flow is one-dimensional and vertical; (2) percolation rate is constant with time; (3) the effect of air convection is negligibly small; (4) thermal conductivity (or diffusivity) is constant for each layer; and (5) the temperature profile does not vary with time. The governing equation for such a heat flow through each layer of the unsaturated zone can be written as:

$$\alpha_{\mathrm{i}} \frac{d^2 T_i}{dz^2} = v \frac{dT_i}{dz} \qquad (i = 1, 2, \cdots, n) \tag{1}$$

where z is the vertical coordinate; T_i is the temperature at an arbitrary point in each layer, °C; v is the percolation flux rate, m/s; α_i is the thermal diffusivity of each layer, m^2/s, which is a constant, defined by

$$\alpha_{\mathrm{i}} = \frac{\lambda_{\mathrm{i}}}{\rho_{\mathrm{w}} \mathrm{c}_{\mathrm{w}}} \qquad (\mathrm{i} = 1,2,\cdots,\mathrm{n}) \tag{2}$$

where ρ_w and c_w are the density (in kg/m^3) and the specific heat capacity (in J/kg·K) of water, respectively; and λ_i is the thermal conductivity (in W/m·K) for each layer. Here the three parameters are treated as constants in the analytical solutions.

The general solution of (1) for each layer is:

$$T_i(z) = C_{i.1} e^{vz/\alpha_i} + C_{i.2} \qquad (i = 1, 2, \cdots, n) \tag{3}$$

where $C_{i.1}$ and $C_{i.2}$ are two integral constants for each layer, and e is the base of natural logarithms.

For convenience, we set $z = 0$ at the surface of the top layer. The z axis is positive downward. If we designate for the base of each layer a depth of d_i, then the thickness of each layer is simply the difference of its two boundary coordinates, and

$$b_i = d_i - d_{i-1} \qquad (i = 1, 2, \cdots, n) \tag{4}$$

where $d_0 = 0$.

Assuming that the temperature at the surface of the top layer is always a known constant, T_0, then

$$T_1(0) = T_0 \tag{5}$$

For the case of constant-temperature lower-boundaries, the boundary condition can be written as

$$T_n(d_n) = T_B \tag{6}$$

where T_B is the known bottom-temperature value of the measured profile.

The integral constants in (3) are as follows (Shan and Bodvarsson 2001):

$$C_{1.1} = \frac{T_B - T_0}{a - 1} \tag{7a}$$

$$C_{1.2} = C_{2.2} = \cdots = C_{n.2} = \frac{aT_0 - T_B}{a - 1} \tag{7b}$$

$$C_{(i+1).1} = e^{vd_i(1/\alpha_i - 1/\alpha_{i+1})} C_{i.1} \qquad (i = 1, 2, \cdots, n-1) \tag{7c}$$

where the parameter, a, introduced for convenience, is defined by

$$a = e^{vd_n/\alpha_{eff}} \tag{8a}$$

where d_n represents the total thickness of the n layers, and α_{eff} is the effective thermal diffusivity of the n layers defined by

$$\alpha_{eff} = d_n / \sum_{i=1}^{n} (b_i / \alpha_i) \tag{8b}$$

As expected, Equation (8b) resembles that of the effective hydraulic conductivity for flow crossing a multi-layered saturated porous medium.

It is of useful to evaluate the conductive and convective heat fluxes from the above solutions. These are given by:

$$F_{conv.} = \rho_w c_w v T_i \tag{9a}$$

$$F_{cond.} = -\lambda_i \left(\frac{dT_i}{dz} \right) \tag{9b}$$

The sum of these two components of the total heat flux is in fact, a constant that is consistent with the assumption of a steady state (Shan and Bodvarsson 2001).

3.2. Application of the Analytical Solution

As a demonstration of the usefulness of the analytical solutions, we analyze the measured temperature profile for borehole SD-12. The analysis is performed using a five-layer model, representing the five major unsaturated hydrologic units at Yucca Mountain: the Tiva Canyon unit, the Paintbrush unit, the Topopah Spring upper unit (TSw 1), the Topopah Spring lower unit (TSw 2), and the Calico Hills unit (CH). The depths to the bases of these layers for borehole SD-12 and the thermal properties used are given in Table 2. Thermal properties in Table 2 were obtained from Brodsky et al. (1997) and the

DOE Reference Information Base (1993) and were also for other boreholes. Our approach first uses the solution, which assumes a constant-temperature boundary condition at the bottom of the measured temperature profile, corresponding to that specific temperature value. The ground-surface temperature is also fixed, and then temperatures calculated for various percolation flux rates are compared with the observed data. The percolation flux that best reproduces the observed temperature profile has a signature of the total heat flux as a combination of the conductive heat flow and the convective heat transport by the percolating water. The goodness of fit is evaluated by minimizing the root mean square error (RMS) of the temperatures for each assumed percolation flux, and this RMS represents the best-case estimate.

Figure 3 shows a comparison of the observed temperature profile for borehole SD-12, the derived analytical solution, and the numerical solution calculated using TOUGH2 (Pruess, 1991). As the figure shows, all the analytical and numerical solutions match the observed data very well.

The observed temperature profile was first matched using the analytical solution, as discussed above, resulting in an RMS versus percolation flux graph shown in Figure 4. This figure clearly shows that a percolation flux of 15 mm/yr best matches the observed data for borehole SD-12. Calculations of the conductive and convective components resulted in a total heat flux of 47 mW/m^2. This heat flux value is consistent with estimates of 40 to ±50 mW/m^2 reported for other boreholes by Sass et al. (1988). The agreement between the temperature data, numerical and analytical solutions (Figure 3)

obtained indicates that both solution methods can be used to analyzing the heat flow problem. In a later section, we will further utilize the TOUGH2 code to examine some of the assumptions and limitations of the analytical solution.

It is of importance to examine the sensitivity of the derived temperature profile to the percolation flux, which is shown in Figure 5 for borehole SD-12. In this figure, the temperature profile shows significant sensitivity to the percolation flux rate. It should, however, be acknowledged that the observed data and analysis contain some uncertainties, including thermal-property variability and uncertainty.

4. Analysis of Borehole Temperature Data

Following the general approach given above, the analytical solution is applied to temperature profiles from other boreholes in and near the UZ model area at Yucca Mountain. Table 3 gives the results of these studies in terms of the optimal percolation flux, the RMS, and the net total heat flux at the base of the UZ for each of the boreholes considered. (The last column, labeled "corrected percolation flux," will be discussed below.) First, the percolation-flux values obtained from the analytical solution are found to vary greatly, from zero to over 60 mm/yr. Second, the RMS also varies significantly from borehole to borehole, from a near-perfect fit with the data for borehole NRG-7 to a rather poor fit for boreholes H-6, G-1, G-2, and G-3. Third, the estimated heat fluxes vary considerably from borehole to borehole, making some of the results more reasonable than others. However, the information from the very simple analytical model provides an

opportunity to sort out important features of heat-transfer processes at Yucca Mountain and to help in determining the important parameter of percolation flux.

4.1. Fault Effects

If we consider just the estimated percolation-flux rates from the analysis and correlate the high-percolation-flux boreholes with the "closeness" to faults, we get a very convincing conclusion. When the percolation fluxes shown in Table 3 are compared with borehole locations shown in Figure 1, we see that almost all of the high-flux-rate boreholes are located on or near major faults and structures. The few exceptions include boreholes UZ-1, SD-12, H-4, and G-1, some of which are located in the high-infiltration areas as estimated by Flint et al. (1996). Some of these and other boreholes may also be affected by strong gas flow or circulation, which will impact temperature profiles. This may be the reason for the apparently anomalous estimates of percolation-flux results around these boreholes. For example, young gas has been found in boreholes NRG-7 and SD-12, and other investigators suggest that gaseous processes causing evaporative/condensive heat-transfer effects may be important within and near faults (Yang et al. 1996). However, there are also some indications that leakage in the borehole instrumentation may have influenced the testing of some of these boreholes—for example, at borehole SD-12 (Yang et al. 1998). Furthermore, more recent C-14 data suggest that the gas in Ghost Dance fault is 2,400 to 4,500 years old (LeCain et al., 2000), indicating gas movement and its history at these locations.

Gas flow in faults can significantly affect the apparent percolation flux inferred from temperature data as reported by Finsterle et al. (1996), based on numerical simulations. They simulated an east-west cross section through boreholes UZ-6 and SD-12 using a coupled moisture, gas, and temperature model. The simulation results in their report show the inferred percolation flux in the Topopah Spring unit for a series of gridblocks extending from east to west with apparent high percolation flux near the Dune Wash and Ghost Dance faults, which is attributed to the effects of gas flow on the temperature profiles. The actual infiltration rate and percolation flux near these faults applied in the model are much less than that inferred from the temperature data.

Because of all of the above, it is uncertain how much the estimated percolation flux by matching temperature distributions for boreholes near faults reflects actual percolation or evaporative processes rather than liquid flow. Therefore we have omitted these estimated values from the "corrected percolation flux" column in Table 3.

4.2. RMS Variance for Individual Boreholes

Figures 6 through 8 show the sensitivity of individual borehole temperature data to the percolation flux, represented as RMS functions. Figure 6 shows the relationship for the deep H- and G- boreholes, Figure 7 for some of the deep WT boreholes, and Figure 8 for some of the shallower NRG, A, and UZ boreholes. It is clear from these figures that the percolation flux can be determined with much more confidence for the deeper boreholes than for the shallower ones. In fact, some of the shallower boreholes show little sensitivity to percolation flux because of the limited data points and limited contrasts in

thermal properties. We conclude from this analysis that the analysis method proposed in this paper is better suited for analyzing data from deep boreholes that have temperature data spanning several thermal units. Because of topographic effects, gaseous flow is more important in shallow boreholes, and this process is neglected in the current model.

Based on the above results, we have modified the estimated percolation-rate values shown in Table 3 (labeled "corrected percolation flux mm/yr"). Estimated values for shallow boreholes have been removed because the temperature data from these boreholes are less reliable for determining percolation flux. The results indicate that the crest boreholes have percolation flux on the order of 5 to 10 mm/yr, with somewhat higher values at boreholes G-1, SD-12, and H-4 (about 15-25 mm/yr) (see Figure 9).

5. Numerical Simulation

The numerical simulation analysis of this section was based directly on the 3-D UZ flow model (Bodvarsson et al., 1997), in which fracture and matrix flow of fluids and heat was handled using a dual-permeability approach. The 3-D model includes effects of possible lateral flow, parameter spatial variability, and faults. The analysis used the nonisothermal steady-state flow solution of the 3-D model with the top boundary (ground surface) and the bottom boundary (water table) described with fixed temperatures using field measurements. The purpose of this analysis was to include more realistic geological layering in the analysis with more variability in the thermal properties and took into account the effects of and multi-dimensional fluid and heat flow as well as faults. The

surface infiltration rate with the numerical analysis was spatially varied according to the base-case infiltration map (Flint et al., 1996). In addition, the spatially varying infiltration rates were adjusted by multiplying and dividing a factor of 3 and 5, respectively, to every source term at surface nodes. The thermal-property data used were those of Brodsky et al. (1997) as expressed in terms of the layering in the UZ Model by Ho (written communication, 1997).

Figures 10 and 11 present two examples of the match between the observed data and those computed by the 3-D numerical model for boreholes SD-12 and H-5, respectively, with different infiltration rates. As the figures show, there is generally good agreement between the observed and simulated temperaturess. Figures 10 and 11 show a comparison of simulated and measured temperatures at boreholes SD-12 and H-5, indicating the sensitivity of vertical temperature distributions relative to net surface infiltration rates. Note that the base-case infiltration has an average of Q = 5 mm/year infiltration rates and is spatially varied. For example, at SD-12, the infiltration rate = 10.7 mm/yr. As shown in Figures 10 and 11, increase or decrease in infiltration rate from the averaged Q by a factor 3 or 5 will not match the observed temperature profile at these two borehole locations. The similar temperature calibration using the 3-D model was performed for 27 other boreholes with good match of observed temperatures. These modeling sensitivity analyses of analytical and numerical simulations may help us to quantify the range of percolation flux in the UZ system.

6. Summary and Conclusions

This work describes a methodology of using subsurface temperature data to estimate percolation flux through unsaturated zones. In particular, we have applied both analytical and numerical models for the evaluation of percolation flux from temperature data from Yucca Mountain. The numerical code TOUGH2 was used to check the analytical solutions as well as to conduct 3-D sensitivity studies. The following conclusions are obtained from this work:

1. The analytical solutions, compared well with the results from numerical simulations for all boreholes tested, provides a simple, but useful tool to analyzing UZ fluid and heat flow.
2. The use of temperature data for the estimation of percolation flux is subject to a greater uncertainty for shallow boreholes. This is especially important at Yucca Mountain, where large gas flows occur at shallow depth and topographic effects become more important.
3. The use of temperature data to determine percolation fluxes for deep boreholes looks very promising, although there are uncertainties because of factors such as gas-flow effects, thermal properties, and lateral flow diversion.
4. Percolation fluxes for deep boreholes generally range from zero to about 20 mm/yr. This range is in good agreement with the range of infiltration rates estimated by Flint et al., 1996.
5. Percolation fluxes estimated for boreholes at or near faults are generally higher than the other boreholes. It is uncertain if these high estimates are because of gas-

flow effects or higher percolation fluxes in the fault zone, which cannot be uniquely determined using temperature data alone.

Acknowledgments

The authors would like to thank P. Dobson and D. Hawkes for their review of the manuscript. Thanks are also due to A. Ritcey and M. Villavert for their help in this work. We would also like to thank the two JCH reviewers, J. Sass and R. Fedors, for their insightful and constructive comments and suggestions for improving the manuscript. This work was supported by the Director, Office of Civilian Radioactive Waste Management, U.S. Department of Energy, through Memorandum Purchase Order EA9013MC5X between Bechtel SAIC Company, LLC and the Ernest Orlando Lawrence Berkeley National Laboratory (Berkeley Lab). The support is provided to Berkeley Lab through the U.S. Department of Energy Contract No. DE-AC03-76SF00098.

References

Bodvarsson, G.S., Bandurraga, T.M., and Wu, Y.S., (Editors), 1997, The Site-Scale Unsaturated Zone Model of Yucca Mountain, Nevada, for the Viability Assessment, . Report LBNL-40396, UC-814, Lawrence Berkeley National Laboratory, Berkeley, California.

Bodvarsson, G.S., Wu, Y.S., and Finsterle, S., 1996. Temperature and heat flow analysis. In G.S. Bodvarsson and T.M. Bandurraga (Editors), Development and Calibration of

the Three-Dimensional Site-Scale Unsaturated-Zone Model of Yucca Mountain, Nevada, Chapter 9. Report LBNL-39315. Lawrence Berkeley National Laboratory, Berkeley, California.

Bredehoeft, J.D. and Papadopulos, I.S., 1965. Rates of vertical groundwater movement estimated from the Earth's thermal profile. Water Resour. Res., 1(2): 325–328.

Brodsky, N.S., Riggins, M., Connolly, J., and Ricci, P., 1997. Thermal Expansion, Thermal Conductivity, and Heat Capacity Measurements for Boreholes UE25 NRG-4, UE25 NRG-5, USW NRG-6, and USW NRG-7/7a. SAND 95-1955. Sandia National Laboratories, Albuquerque, New Mexico.

DOE (U.S. Department of Energy), 1997. Yucca Mountain Site Characterization Project Site Atlas 1997. U.S. Department of Energy, Washington, D.C.

DOE, 1993. RIB (Reference Information Base). YMP/93-02m /Rev. 3. U.S. Department of Energy, Yucca Mountain Site Characterization Office, Las Vegas, Nevada.

Finsterle, S., Bandurraga, T.M., Doughty, C., and Bodvarsson, G.S., 1996. Simulation of coupled processes in a two-dimensional west-east cross section of Yucca Mountain, Nevada." In: G.S. Bodvarsson and T.M. Bandurraga (Editors), Development and Calibration of the Three-Dimensional Site-Scale Unsaturated-Zone Model of Yucca

Mountain, Nevada, Chapter 12. Report LBNL-39315. Berkeley, California: Lawrence Berkeley National Laboratory, Berkeley, California.

Flint, A. L., Hevesi, J. A. and Flint, E. L*., Conceptual and Numerical Model of infiltration for the Yucca Mountain Area, Nevada*, U. S. Geological Survey, Water-Resources Investigation Report-96, Denver, Colorado, 1996.

Fridrich, C.J.; Dudley, W.W., Jr.; and Stuckless, J.S., 1994. Hydrogeologic analysis of the saturated-zone groundwater system, under Yucca Mountain, Nevada. *Journal of Hydrology, 154*: 133–168.

LeCain, G.D., Anna, L.O., and Fahy, M.F., 2000. Results from Geothermal Logging, Air- and Core-Water Chemistry Sampling Air-Injection Testing, and Tracer Testing in the Northern Ghost Dance Fault, Yucca Mountain, Nevada, November 1996 to August 1998. U.S. Geological Survey Water-Resources Investigations Report 99-4210. U.S. Geological Survey, Denver, Colorado.

Luckey, R.R., 1996. Related Data Water-Level, Discharge Rate and from the Pump Tests Conducted at Well USW UZ-14, August 17 through August 30, 1993. Denver, Colorado: U.S. Geological Survey.

Pruess, K., 1991. TOUGH2—A General Purpose Numerical Simulator for Multiphase Fluid and Heat Flow. Report LBL-29400. Lawrence Berkeley National Laboratory, Berkeley, California.

Rautman, C.A. and Engstrom, D.A., 1996. Geology of the USW SD-12 Drill Hole, Yucca Mountain, Nevada. SAND96-1368. Sandia National Laboratories, Albuquerque, New Mexico.

Rousseau, J.P., Kwicklis, E.M., and Gillies, D.C. (Editors), 1999. Hydrogeology of the Unsaturated Zone, North Ramp Area of the Exploratory Studies Facility, Yucca Mountain, Nevada, USGS-WRIR-98-4050. Submitted for publication as a Water-Resources Investigations Report. U.S. Geological Survey, Denver, Colorado.

Sass, J.H. and Lachenbruch, A.H., 1982. Preliminary Interpretation of Thermal Data from the Nevada Test Site. U.S. Geological Survey Open-File Report 82-973. U.S. Geological Survey, Denver, Colorado.

Sass, J.H., Lachenbruch, A.H., Dudley, Jr., W.W., Priest, S.S., and Munroe, R.J. 1988. Temperature, Thermal Conductivity and Heat Flow near Yucca Mountain, Nevada: Some Tectonic and Hydrologic Implications. U.S. Geol. Surv. Open File Rep. 87-649. U.S. Geological Survey, Denver, Colorado.

Shan, C.; and Bodvarsson, G.S., 2001. A new analytical method for evaluating percolation flux from temperature profiles from boreholes. To be submitted to the *Journal of Heat Transfer*.

Tucci, P. and Burkhardt, D.J., 1995. Potentiometric-Surface Map, 1993, Yucca Mountain and Vicinity, Nevada. Water-Resources Investigations Report 95-4149. U.S. Geological Survey, Denver, Colorado.

Wu, Y.S., Ritcey, A.C., and Bodvarsson, G.S., 1998. A modeling study of perched water phenomena in the vadose zone." J. Contamin. Hydrol. 38(1-3): 157–184.

Yang, I.C., Rattray, G.W., and Yu, P., 1996. Interpretations of Chemical and Isotopic Data from Boreholes in the Unsaturated-Zone at Yucca Mountain, Nevada. U.S. Geological Survey Water-Resources Investigation Report 96-4058. U.S. Geological Survey, Denver, Colorado.

Yang, I.C., Yu, P., Rattray, G.W., Ferarese, J.S., and Ryan, J.N., 1998. Hydrochemical Investigations in Characterizing the Unsaturated Zone at Yucca Mountain, Nevada. U.S. Geological Survey Investigations Report 98-4132. U.S. Geological Survey, Denver, Colorado.

Figure Captions

Figure 1. Map showing the borehole locations used for the present study, the study area of the 3-D, Unsaturated-Zone Site-Scale Flow and Transport Model, and surface traces of identified faults.

Figure 2. Heat-flow distribution in the unsaturated zone (mW/m^2) taken from Sass et al. (1988).

Figure 3. Comparison of the observed and calculated temperature profiles at borehole SD-12.

Figure 4. The relationship between percolation flux and RMS for borehole SD-12.

Figure 5. Sensitivity of derived temperature profiles using the analytical solution to percolation flux for borehole SD–12.

Figure 6. Root-mean-square error versus percolation flux for G-and H- boreholes.

Figure 7. Root-mean-square error versus percolation flux for WT- and SD-12 boreholes.

Figure 8. Root-mean-square error versus percolation flux for selected A-, NRG-, and UZ-boreholes.

Figure 9. Locations of boreholes and estimated values of percolation flux in mm/yr.

Figure 10. Comparison between modeled (3-D model) and observed temperature data for borehole SD-12 with different net infiltration rates.

Figure 11. Comparison between modeled (3-D model) and observed temperature data for borehole H-5 with different net infiltration rates.

Table Captions

Table 1. Location, elevation, and completion information for the selected boreholes.

Table 2. Thermal properties used for different layers in analytical analysis.

Table 3. Results of analytical study of temperatures.

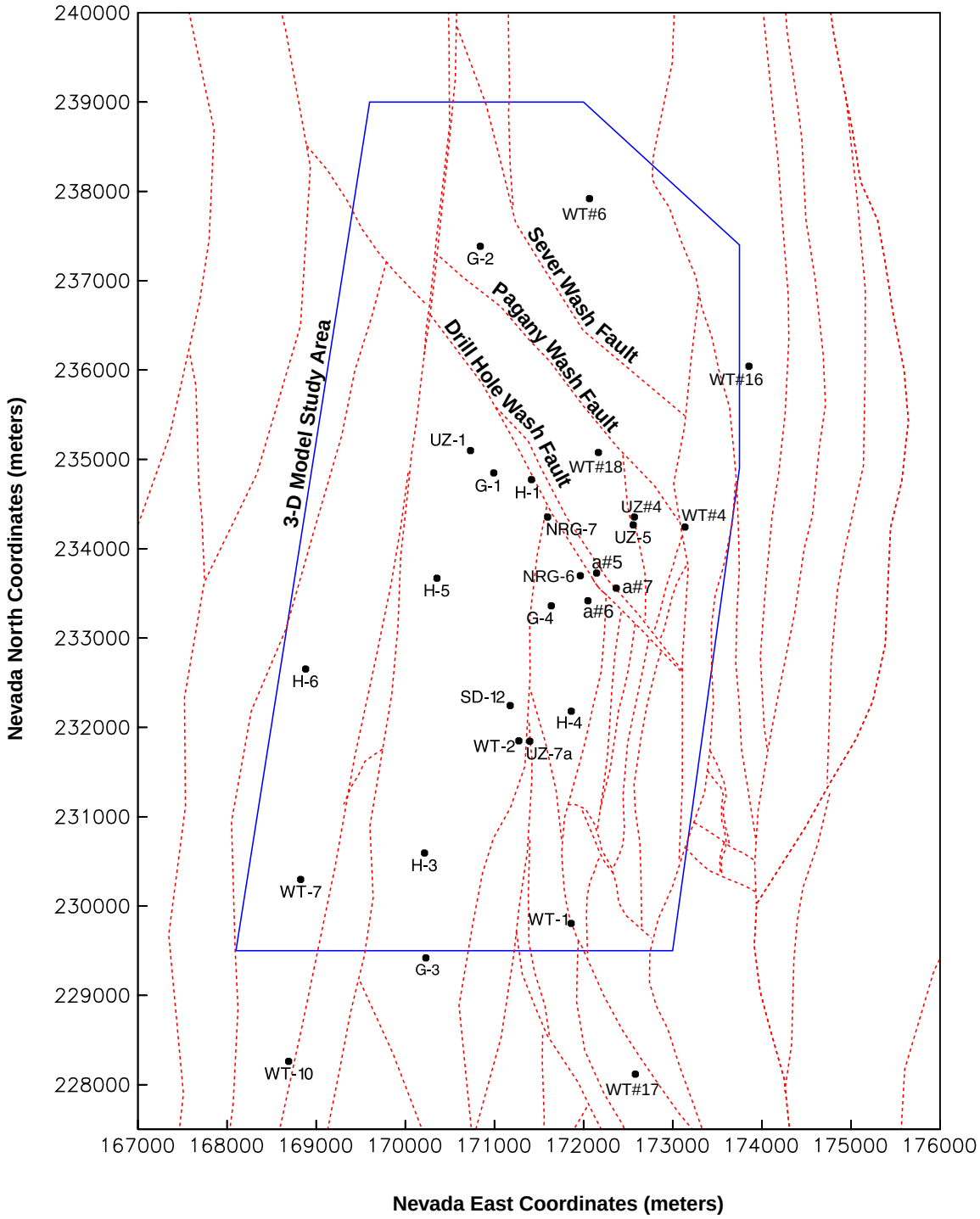
240000
239000
238000
237000
236000
235000
234000
233000
232000
231000
230000
229000
228000
Nevada North Coordinates (meters)
167000
168000
169000
170000
171000
172000
173000
174000
175000
176000
Nevada East Coordinates (meters)
3-D Model Study Area
Drill Hole Wash Fault
Pagany Wash Fault
Sever Wash Fault
WT#6
G-2
WT#16
UZ-1
WT#18
G-1
H-1
UZ#4
WT#4
NRG-7
UZ-5
a#5
NRG-6
a#7
H-5
G-4
a#6
H-6
SD-12
H-4
WT-2
UZ-7a
H-3
WT-7
WT-1
G-3
WT-10
WT#17

Figure 1.

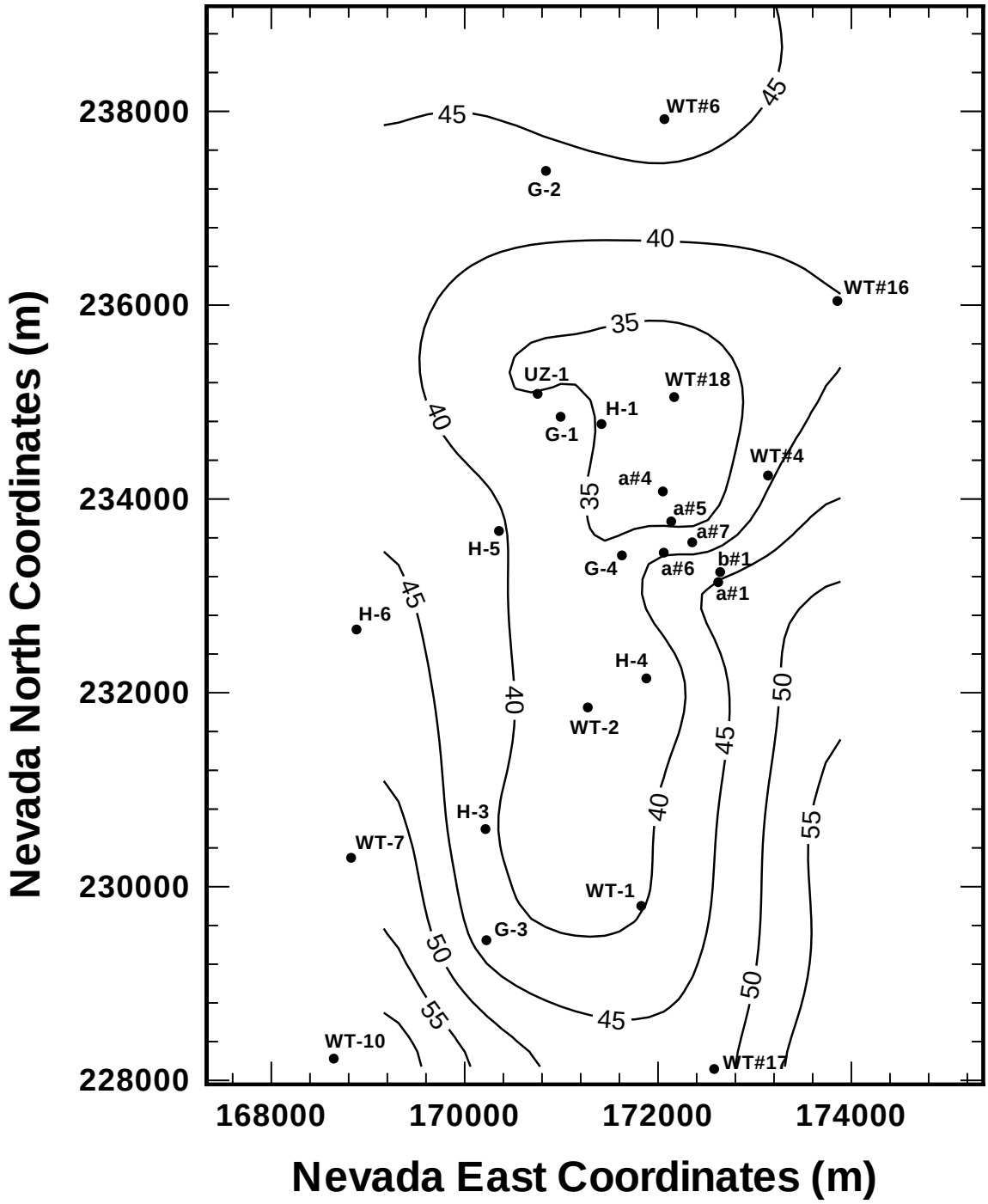
Nevada North Coordinates (m)
238000
236000
234000
232000
230000
228000
168000
170000
172000
174000
Nevada East Coordinates (m)
WT#6
G-2
WT#16
UZ-1
WT#18
H-1
G-1
WT#4
a#4
a#5
a#7
H-5
G-4
a#6
b#1
a#1
H-6
H-4
WT-2
H-3
WT-7
WT-1
G-3
WT-10
WT#17
45
40
35
50
55

Figure 2.

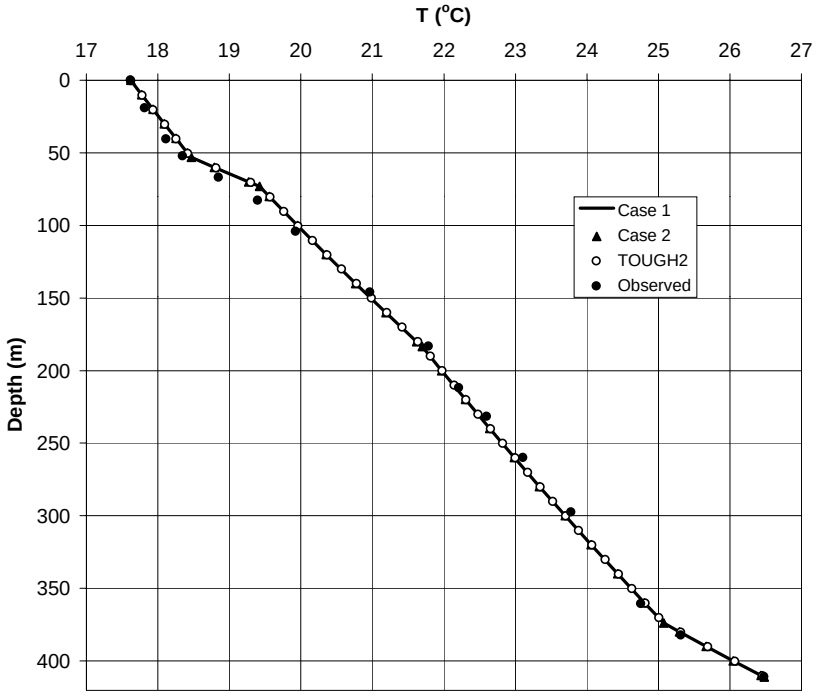
T (°C)
17
18
19
20
21
22
23
24
25
26
27
0
50
100
150
200
250
300
350
400
Depth (m)
Case 1
Case 2
TOUGH2
Observed

Figure 3.

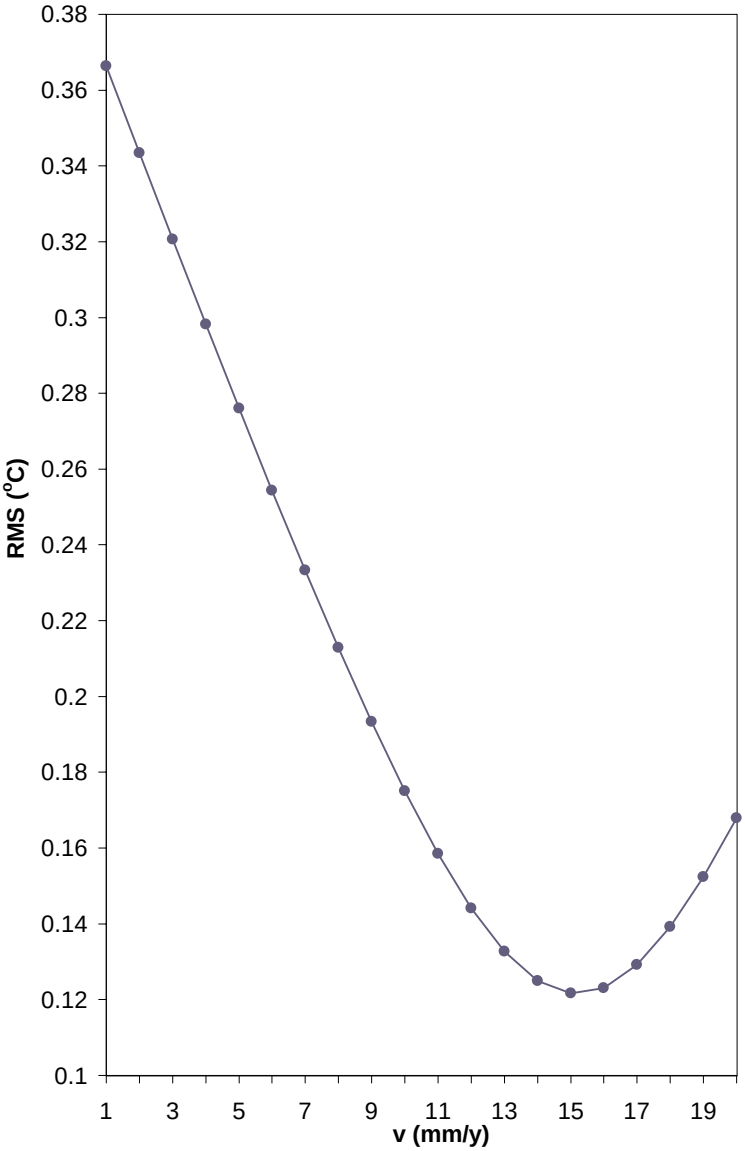
0.38
0.36
0.34
0.32
0.3
0.28
0.26
0.24
0.22
0.2
0.18
0.16
0.14
0.12
0.1
RMS (°C)
1
3
5
7
9
11
13
15
17
19
v (mm/y)

Figure 4.

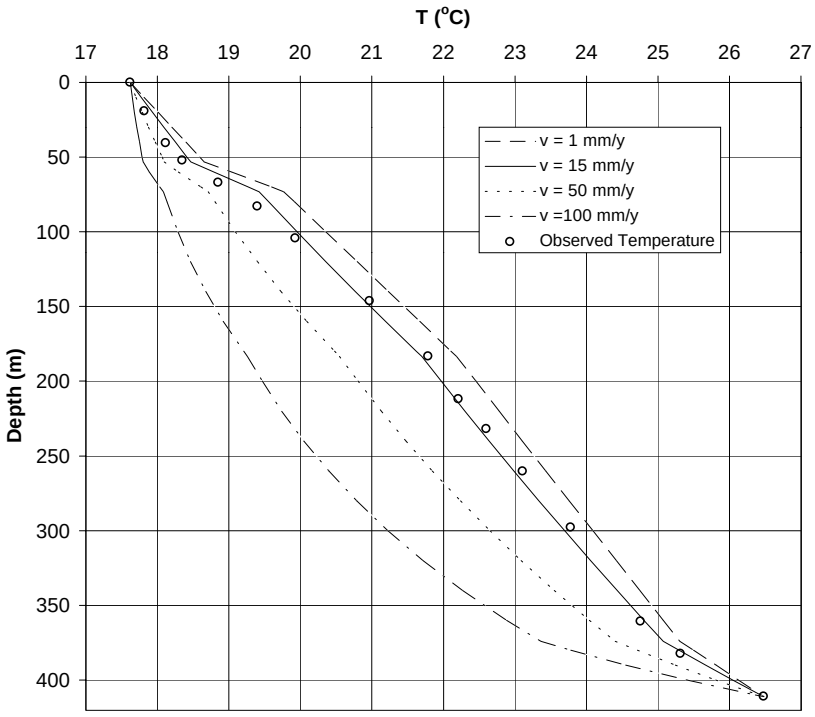
T (°C)
17
18
19
20
21
22
23
24
25
26
27
0
50
100
150
200
250
300
350
400
Depth (m)
v = 1 mm/y
v = 15 mm/y
v = 50 mm/y
v =100 mm/y
Observed Temperature

Figure 5.

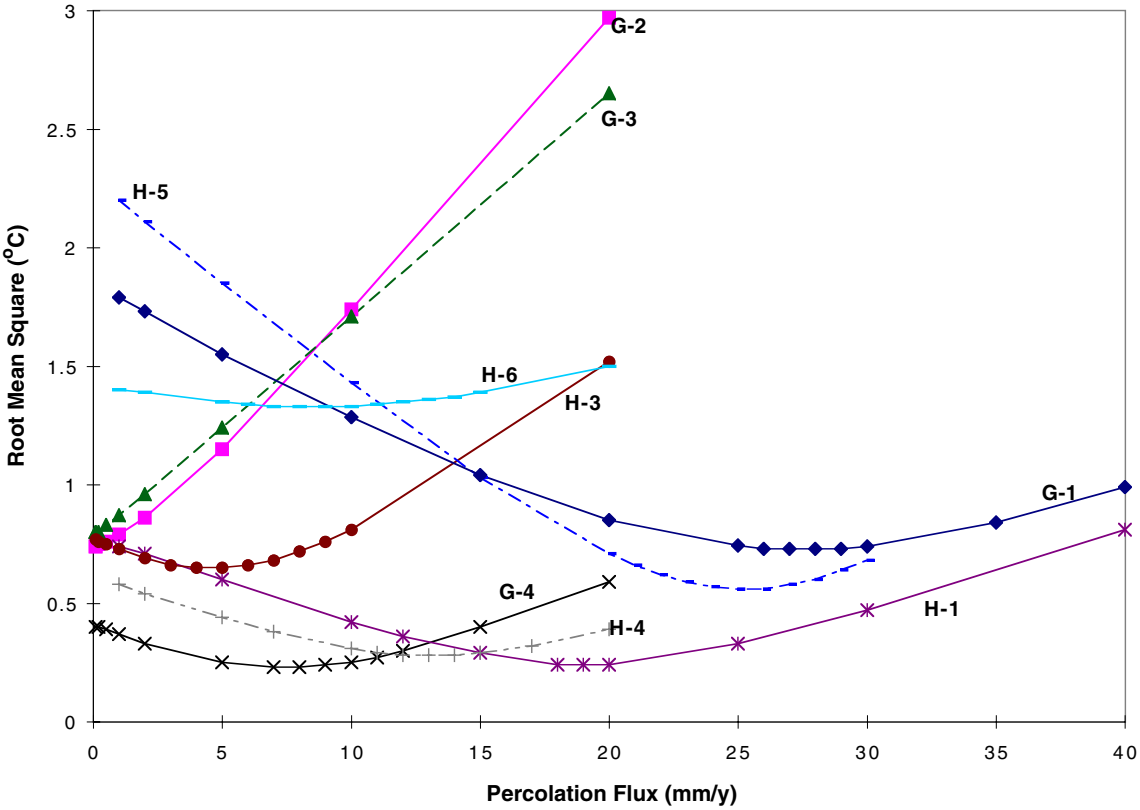
Root Mean Square (°C)
Percolation Flux (mm/y)
G-2
G-3
H-5
H-6
H-3
G-1
G-4
H-4
H-1
0
0.5
1
1.5
2
2.5
3
0
5
10
15
20
25
30
35
40

Figure 6.

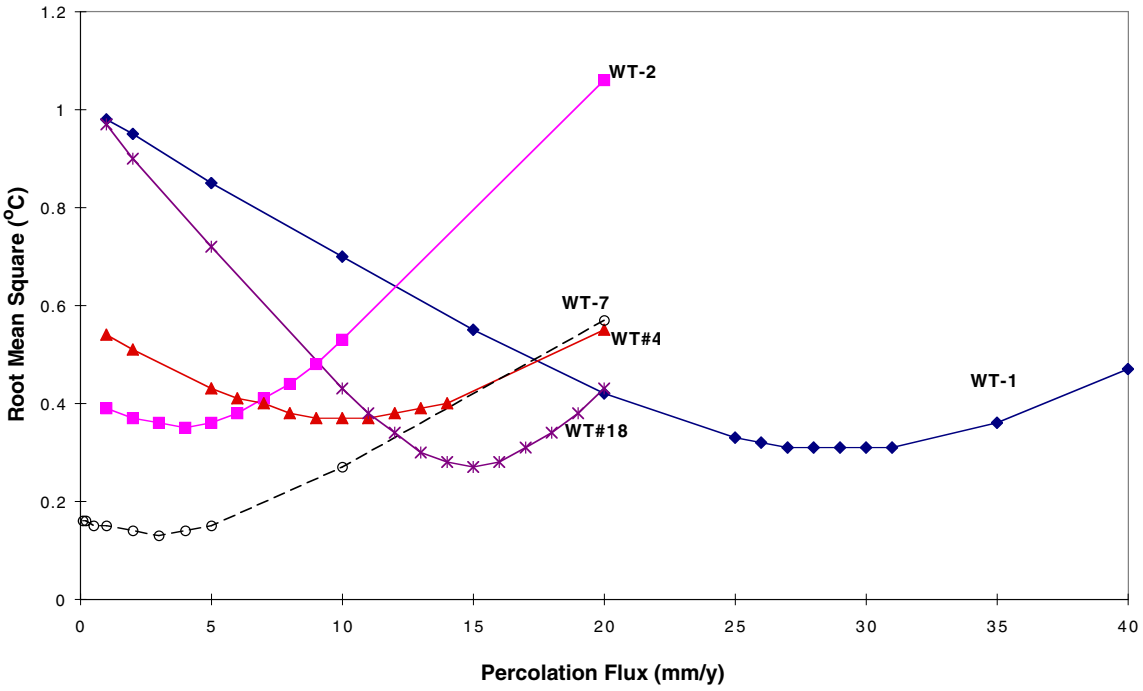
1.2
1
0.8
0.6
0.4
0.2
0
Root Mean Square (°C)
0
5
10
15
20
25
30
35
40
Percolation Flux (mm/y)
WT-2
WT-7
WT#4
WT-1
WT#18

Figure 7.

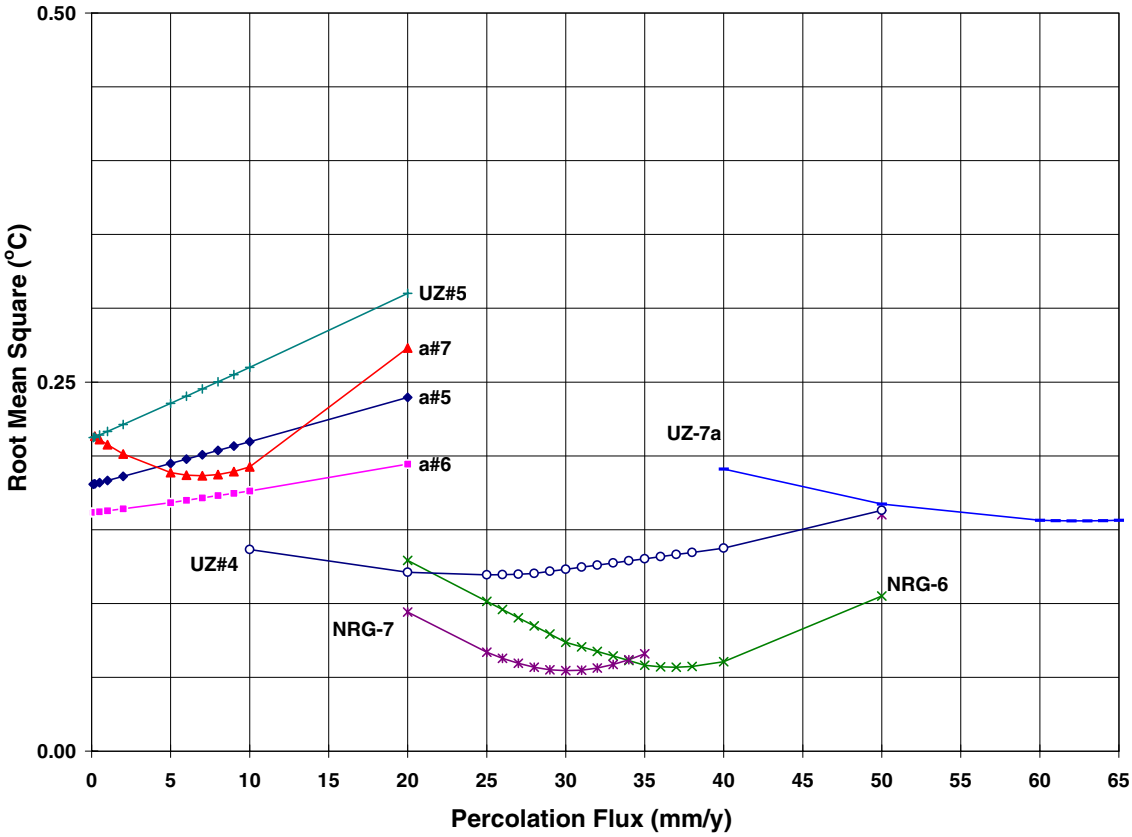
0.50
0.25
0.00
Root Mean Square (°C)
0
5
10
15
20
25
30
35
40
45
50
55
60
65
Percolation Flux (mm/y)
UZ#5
a#7
a#5
a#6
UZ-7a
UZ#4
NRG-7
NRG-6

Figure 8.

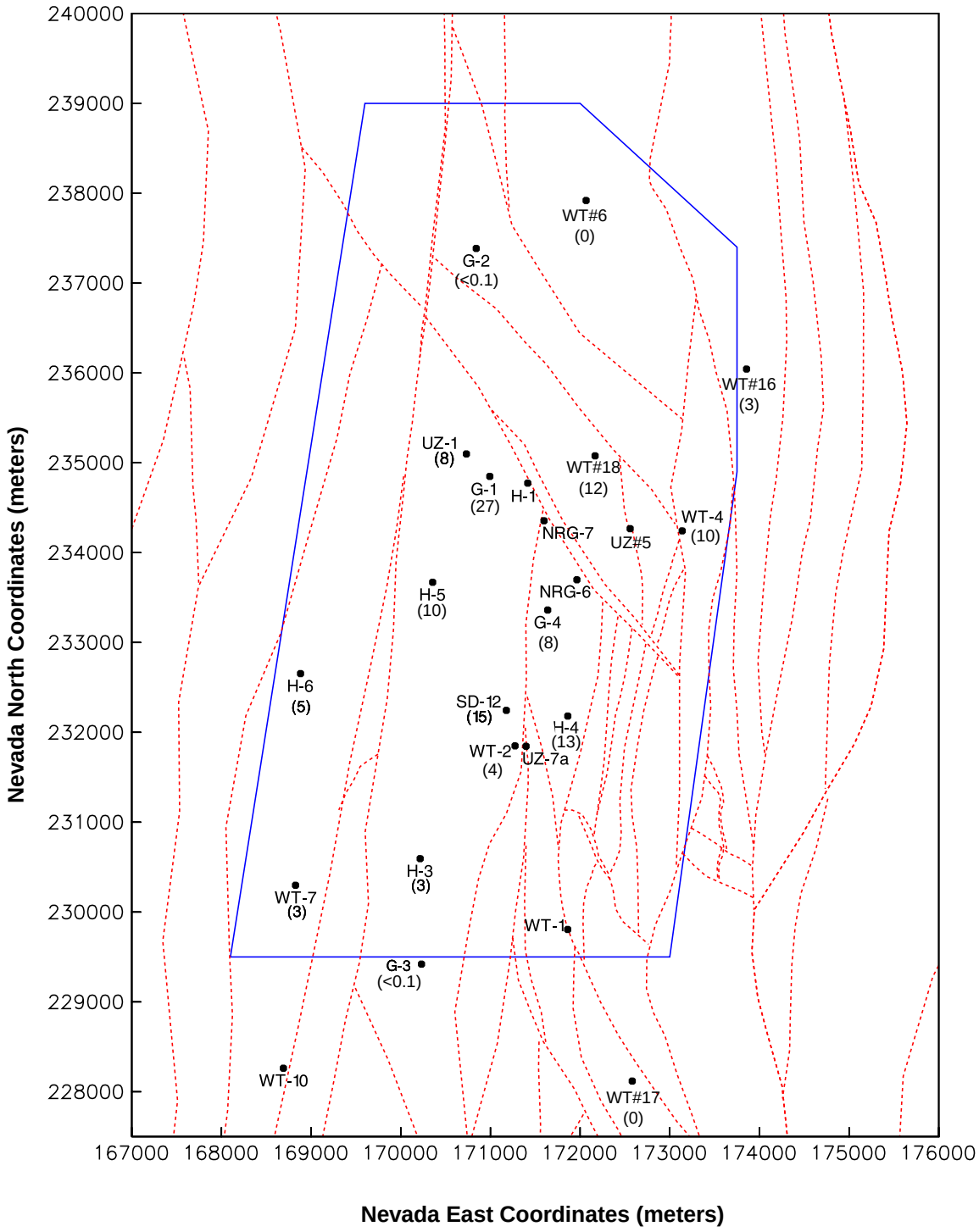
Nevada North Coordinates (meters)
Nevada East Coordinates (meters)
240000
239000
238000
237000
236000
235000
234000
233000
232000
231000
230000
229000
228000
167000
168000
169000
170000
171000
172000
173000
174000
175000
176000
WT#6
(0)
G-2
(<0.1)
WT#16
(3)
UZ-1
(8)
WT#18
(12)
G-1
(27)
H-1
NRG-7
UZ#5
WT-4
(10)
H-5
(10)
NRG-6
G-4
(8)
H-6
(5)
SD-12
(15)
H-4
(13)
WT-2
(4)
UZ-7a
H-3
(3)
WT-7
(3)
WT-1
G-3
(<0.1)
WT-10
WT#17
(0)

Figure 9.

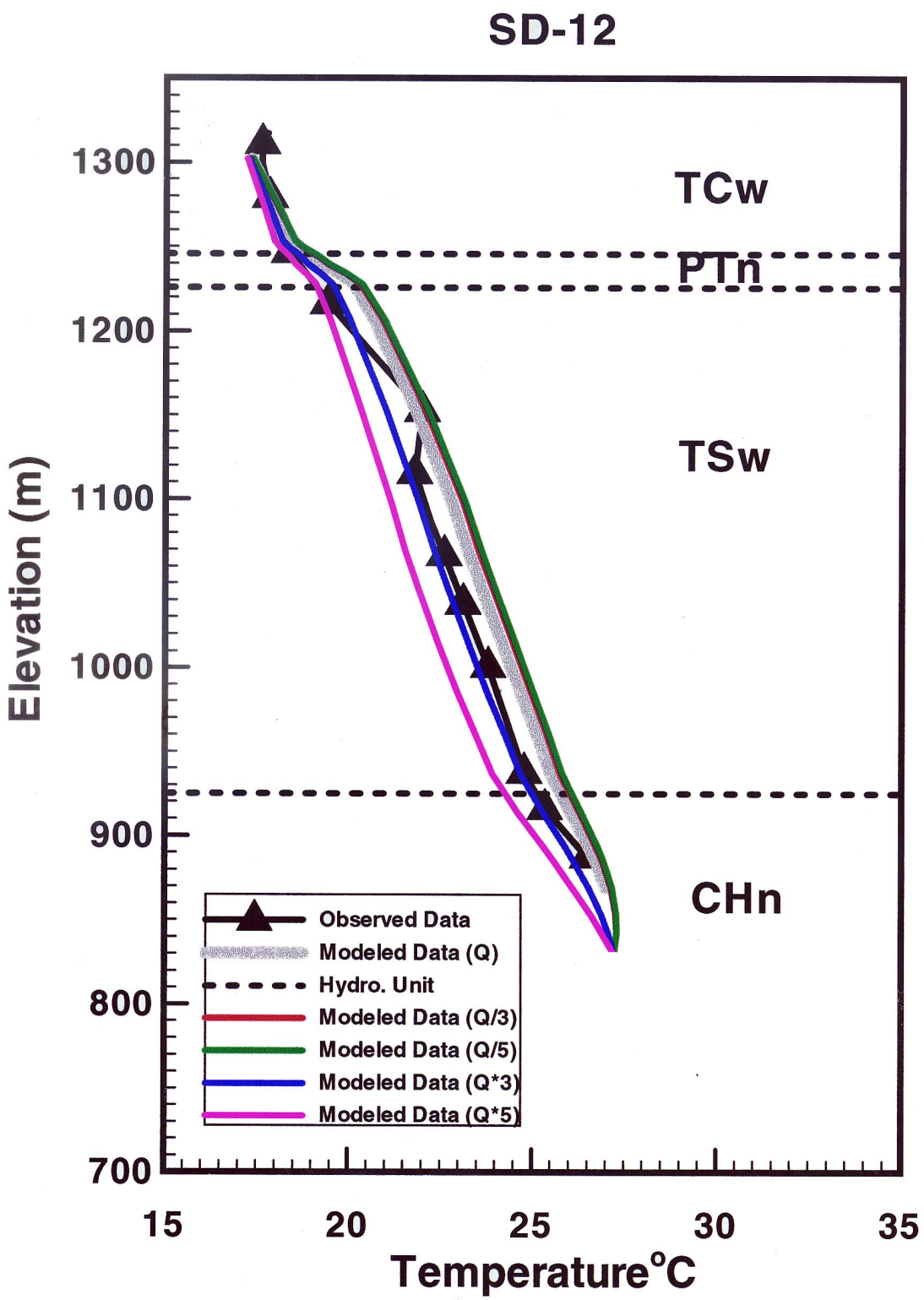
SD-12
1300
1200
1100
1000
900
800
700
Elevation (m)
TCw
PTn
TSw
CHn
Observed Data
Modeled Data (Q)
Hydro. Unit
Modeled Data (Q/3)
Modeled Data (Q/5)
Modeled Data (Q*3)
Modeled Data (Q*5)
15
20
25
30
35
Temperature°C

Figure 10.

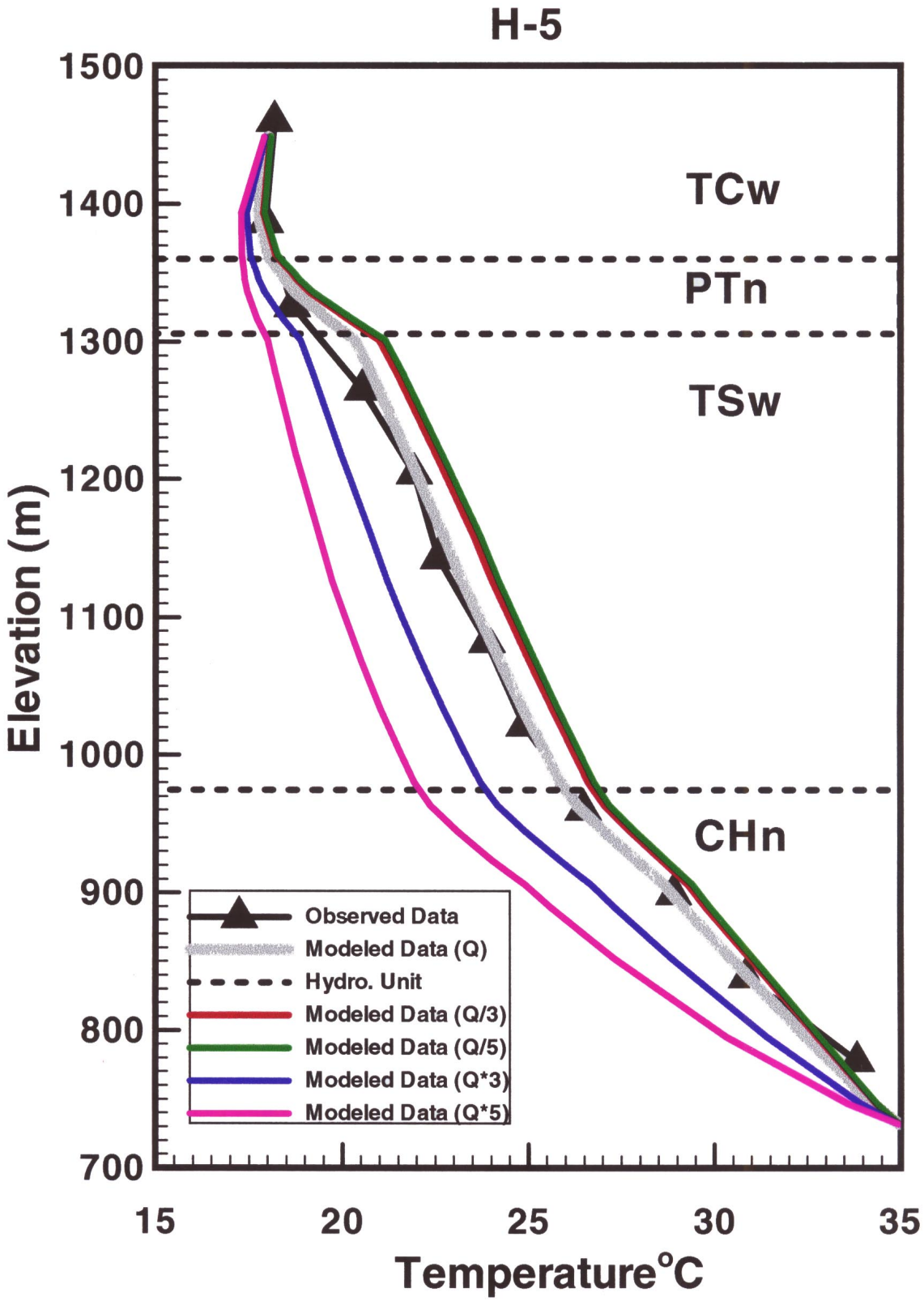
H-5
1500
1400
1300
1200
1100
1000
900
800
700
Elevation (m)
TCw
PTn
TSw
CHn
Observed Data
Modeled Data (Q)
Hydro. Unit
Modeled Data (Q/3)
Modeled Data (Q/5)
Modeled Data (Q*3)
Modeled Data (Q*5)
15
20
25
30
35
Temperature°C

Figure 11.

Table 1. Location, elevation, and completion information for the selected boreholes

Borehole Designation	Borehole Coordinates (m)[1]		Elevation (m)	Total Depth (m)	Water Level Elevation (m)
	North	East			
a#1	233142	172623	1199[5]	762[5]	730[5]
a#4	234078	172051	1277[3]	152[5]	na[2]
a#5	233768	172137	1234[3]	148[5]	na[2]
a#6	233446	172060	1231[3]	152[5]	na[2]
a#7	233553	172355	1219[3]	305[5]	na[2]
b#1	233246	172644	1201[6]	1220[6]	731[2]
G-1	234848	170993	1326[3]	1829[5]	750[2]
G-2	237386	170842	1554[3]	1831[6]	1020[2]
G-3	229447	170226	1480[3]	1533[6]	730[2]
G-4	233418	171627	1270[3]	915[5]	731[2]
H-1	234773	171416	1302[3]	1829[6]	731[2]
H-3	230594	170216	1483[3]	1219[6]	731[2]
H-4	232149	171880	1249[3]	1219[6]	730[2]
H-5	233670	170355	1478[3]	1219[6]	776[2]
H-6	232654	168882	1302[3]	1220[6]	776[2]
WT-1	229801	171828	1202[3]	515[6]	731[3]
WT-2	231849	171274	1301[3]	628[6]	730[3]
WT#4	234242	173139	1167[3]	482[6]	728[3]
WT#6	237920	172067	1313[3]	383[6]	1035[2]
WT-7	230298	168826	1197[3]	491[6]	779[2]
WT-10	228225	168646	1123[3]	431[6]	775[3]
WT#16	236043	173856	1210[3]	521[6]	738[2]
WT#17	228118	172581	1124[3]	443[6]	729[3]
WT#18	235052	172168	1336[3]	623[6]	731
UZ-1	235085	170755	1349[5]	384[5]	na
UZ#4	234305	172559	1201[5]	112[5]	na[2]
UZ#5	234267	172558	1205[5]	111[5]	na[2]
UZ-7a	231914**	171584**			
NRG-6	233698	171964	1248[5]	335[5]	na
NRG-7	234344	171604	1282[5]	461[5]	822
NRG-7a	234355	171598	1282[5]	461[5]	822
SD-12	232244	171178	1324[4]	660[4]	730[4]

[1]from DOE, 1997
[2]from Luckey, 1996
[3]from Sass et al., Table 2, 1988
[4]from Rautman and Engstrom, Geology of SD-12, 1996
[5]from CRWMS M&O, 1996
[6]from Tucci and Burkhardt, 1995
** number for UZ-7, not UZ-7a

Table 2. Thermal properties used for different layers in analytical analysis

Layer Unit	Thermal Conductivity (W/m•K)	Thermal Diffusivity (m^2/s)	Depth to Base of Layer (m)
1. Tiva Canyon	1.89	4.52×10^{-7}	53.21
2. Paintbrush	0.66	1.58×10^{-7}	73.09
3. Topopah Spring I	1.70	4.07×10^{-7}	183.49
4. Topopah Spring II	2.29	5.48×10^{-7}	373.99
5. Calico Hills	1.20	2.87×10^{-7}	411.17

Table 3. Results of analytical study of temperatures

Borehole	Analytical Percolation Flux (mm/yr)	RMS (°C)	Heat Flux (mW/m^2)	Corrected Percolation Flux (mm/yr)
a#5	0	0.18	32	–
a#6	0	0.16	34	–
a#7	7	0.19	42	7
G-1	27	0.73	47	27
G-2	<0.1	0.75	25	<0.1
G-3	<0.1	0.80	36	<0.1
G-4	8	0.23	42	8
H-1	19	0.24	43	–
H-3	5	0.65	36	5
H-4	13	0.28	45	13
H-5	25	0.56	66	10
H-6	8	1.33	54	5
NRG-6	37	0.06	41	–
NRG-7	30	0.05	40	–
SD-12	15	0.12	47	15
UZ-1	8	0.05	45	8
UZ#4	25	0.12	34	–
UZ#5	0	0.21	37	–
UZ-7a	63	0.16	50	–
WT-1	29	0.31	69	–
WT-2	4	0.36	41	4
WT#4	10	0.38	48	10
WT#6	0	0.24	36	0
WT-7	3	0.14	56	3
WT-10	15	0.28	42	–
WT#16	3	0.74	41	3
WT#17	0	0.50	46	0
WT#18	12	0.35	40	12